13th International Symposium on Turbulence and Shear Flow Phenomena (TSFP13)
Montreal, Canada, June 25–28, 2024

MODAL DECOMPOSITION OF HIGH-SPEED CAVITY FLOWS USING NON-TIME-RESOLVED PIV AND QUANTITATIVE SCHLIEREN

Yang Zhang
Mechanical, Materials, and Aerospace Engineering
Illinois Institute of Technology
Chicago, IL, US
yzhang215@iit.edu

Louis Cattafesta
Mechanical, Materials, and Aerospace Engineering
Illinois Institute of Technology
Chicago, IL, US

Lawrence Ukeiley
Mechanical and Aerospace Engineering
University of Florida
Gainesville, FL, US

Kunihiko Taira
Mechanical and Aerospace Engineering
University of California
Los Angeles, CA, US

ABSTRACT

Cavity flow oscillations induced by high-speed flows are encountered in many engineering applications. Open cavity flows are associated with strong fluctuations of velocity/pressure with both tonal and broadband content. To study the dynamics of high-speed cavity flows, time-resolved velocity/pressure measurements can be obtained using high-speed optical methods or sensors. To study compressibility effects relating velocity/pressure coupling of high subsonic cavity flows, time-resolved Particle Image Velocimetry (PIV) and density measurements can be utilized. However, the equipment for time-resolved optical measurements is often cost-prohibitive, and high-speed cameras have relatively low resolution. In our previous study (Zhang *et al.*, 2020), we developed a spectral analysis modal method (SAMM) to obtain the dynamics of the velocity field from synchronized non-time-resolved PIV and time-resolved surface pressure measurements for the cavity flow at Mach 0.6. In addition to the SAMM method on the PIV and surface-pressure data, we utilize the same method to obtain the correlation between the density field obtained from quantitative Schlieren and time-resolved surface pressure measurements of the same cavity flow at Mach 0.6. The reduced order modeling of velocity and density fields are consequentially linked using the surface pressure. The results quantify the relationship between the density and pressure with the coherent vortical structures in the flow field at the Rossiter frequencies.

Introduction

Flow over open cavities represents a fundamental class of flows dominated by feedback resonant phenomena (Rossiter, 1964; Tam & Block, 1978; Rockwell & Naudascher, 1978). From an applied perspective, flows over open cavities exist on many military aircraft in weapons bays and wheel wells. The associated oscillations are often detrimental to aircraft operations. Cavity flows are characterized by velocity and pressure spectra with broadband and tonal components. In cavity flows, the fluctuating surface pressures are driven by the fluid-acoustic interaction between the shear layer emanating from the leading edge and the acoustic source at the aft wall of the cavity due to the shear layer impingement. This feedback loop results in characteristic intense tonal peaks, often referred to as Rossiter modes (Rossiter, 1964).

Generally speaking, the frequency of these modes is on the order of kHz in small-scale wind tunnel models at subsonic or supersonic speeds. Both time-resolved PIV and Schlieren/shadowgraph are feasible to obtain the dynamics of the quantitative velocity and semi-quantitative spanwise-averaged density fields. While time-resolved velocity fields can be obtained from PIV measurements, time-resolved measurements of density fields to study compressibility effects are still challenging in high-speed cavity flows. The limitations are the high sampling rate to satisfy the Nyquist criterion and the short exposure time to ‘freeze’ the flow. In addition, the resolution and dynamic range of high-speed cameras also impose limitations. We conducted simultaneous time-resolved PIV, Schlieren, and surface-pressure measurements in our previous attempt. Although the velocity measurements were successful, the seeding particles contaminated the Schlieren measurements. Therefore, the PIV and Schlieren measurements have to be performed independently.

The idea of recovering time-resolved data using synchronized non-time-resolved and time-resolved measurements is not new, for example, variants of stochastic estimation (linear, quadratic, or spectral) (Adrian, 1979; Murray & Ukeiley, 2003; Taylor & Glauser, 2004; Tinney *et al.*, 2006; Durgesh & Naughton, 2010). These methods generally aim to recover the data in the time domain. In Zhang *et al.* (2020), the modal decomposition method is directly performed in the frequency domain, in which the dynamically coherent velocity modes calculated from a low sampling rate (15 Hz) PIV agreed with the time-resolved PIV measurements sampled at 16 kHz. The method is based on obtaining velocity and pressure correlations combined with conditional spectral analysis. Therefore, to study the dynamics of the density field, we perform synchronized low sampling rate quantitative Schlieren and time-resolved surface pressure measurements to obtain the coupling between the density field and surface fluctuating pressure. The surface-pressure measurements, common to both measurements, then serve as a 'bridge' to link the dynamics of the velocity field and the density flow field.

Experimental Setup

The experiments were carried out at the Florida Center for Advanced Aero-Propulsion at Florida State University. The details of the wind tunnel facility and the cavity model can be found in Zhang *et al.* (2020). In brief, the cavity model has a dimension of $L/D = 6$ and full-span width $W/D = 3.85$, and the flow condition is Mach 0.6. The experimental arrangement in the current study includes two setups, i.e., PIV (Figure 1a) or Schlieren (Figure 1b), both with synchronous surface fluctuating pressure measurements.

Two-component, planar PIV is performed to obtain the streamwise flow field in the $(\tilde{x}-\tilde{y})$ plane along the center plane of the cavity. A double-pulse Evergreen Nd:YAG laser (EVG00200) produces laser pulses at a repetition rate of 15 Hz. The beams travel through a series of optics and pass through the transparent cavity floor, resulting in a laser sheet with a thickness of approximately 1.5 mm. The sheet illuminates seeding particles injected upstream of the stagnation chamber using Rosco fog fluid. One Imager sCMOS camera with 2560×2160 pixels, equipped with a Nikon 105 mm lens and a 532 nm bandpass filter, is oriented with its optical axis normal to the laser sheet. Calibration is performed using a LaVision 3D target prior to the measurements. A total number of 5959 snapshots are acquired. Data processing is performed using a multipass scheme with a window size ranging from 128×128 to 32×32 pixels and a 75% overlap in DaVis 8.4. The data are post-processed to remove the outliers first in the DaVis software and then using multi-variate outlier detection (Griffin *et al.*, 2010) in Matlab. The removed outlier vectors are filled using a Proper Orthogonal Decomposition (POD)-based gappy-PIV method (Venturi & Karniadakis, 2004; Murray & Ukeiley, 2006). The resulting vector resolution is approximately 2 vectors/mm.

A conventional Z-type Schlieren is used to visualize the density gradient field. The light from the pulsed customized LED passes through a $F/2$ ⌀50 mm achromatic lens to focus on a rectangular slit. The light diverges onto the first $F/6$ ⌀320 mm parabolic mirror to produce a collimated beam. Two surface mirrors pass the collimated beam through the test section to the second parabolic mirror. The parabolic mirror directs the light beam on a horizontal knife edge, followed by a Prosilica GT 4905 camera. During the experiments, the Schlieren LED is triggered for 5 μs exposure time at a repetition rate of 13 Hz.

In order to obtain quantitative results, the knife edge cut-off is calibrated before the measurements (Garg & Cattafesta III, 2001). The knife edge is set horizontally; hence the density gradient of the flow field in the vertical direction $(\partial\rho/\partial\tilde{y})$ is captured. The knife edge is traversed vertically and the images progress from dark to bright. The Schlieren image at each knife edge vertical location is recorded. A linear fit is used to obtain the relationship between the light intensity and the knife edge location for each pixel, and an example is shown in Figure 2a. For each instantaneous image, the pixel intensities are converted to the deflection of light based on the calibration. Using the Gladstone-Dale law and geometrical optics, the density gradient in the vertical direction can be calculated via

$$\frac{\partial\rho}{\partial\tilde{y}} \approx \frac{\Delta\tilde{y}}{f_{\mathrm{focal}}kW}, \tag{1}$$

where $\Delta\tilde{y}$ is the light deflection in the vertical direction, f_{focal} is the parabolic mirror focal length, k is the Gladstone-Dale constant, and W is the test section width. The density of the compressible flow at Mach 0.6 is first calculated using the isentropic equations and the ideal gas law with measured P_o, P_s, and T_0. Assuming the time-averaged density is constant in the freestream at the top boundary, the density field is obtained by integrating from the top boundary to the bottom of the cavity. Figure 2b shows an example of the resulting instantaneous density field, in which the wavy shear layer and the large density gradient near the cavity trailing edge vicinity are well resolved. A total number of 8125 density snapshots are obtained.

In both experiments, the surface fluctuating pressure data from 3 Kulite sensors are acquired simultaneously at a sampling rate of 25.6 kHz using an NI-4462 card. Three Kulite sensors (two XTE190 and one XT190) are located at front floor (FF, $\tilde{x}$=1.5), aft floor (AF, $\tilde{x} = 4.5$), and middle of aft wall (AW), respectively. The laser pulse signal is captured by a photodetector in the PIV measurement, while the LED trigger is recorded in the Schlieren experiment along with the unsteady pressure data simultaneously, a critical step for the SAMM technique (Zhang *et al.*, 2020).

1 Methodology

Details of the SAMM algorithm is provided in Zhang *et al.* (2020). The current paper adopts the same terminology, where x is the pressure input while y is the velocity/density output. For the multi-input/multi-out (MIMO) model in the frequency domain, we have

$$\hat{G}_{y_iy_j} = HG'_{x_ix_j}H', \tag{2}$$

where $\hat{G}_{y_iy_j}$ is the estimated cross-spectral density of the outputs, H is the transfer function of the MIMO system, and $G'_{x_ix_j}$ is the complex conjugate of the cross-spectral density of the inputs. The procedure for computing the cross-spectral density matrix and the transfer function is detailed in Zhang *et al.* (2020), which are achieved by performing discrete Fourier transform on the cross-correlation R_{xy} between inputs and outputs and the cross-correlation $R_{x_ix_j}$ between inputs. Because $G_{x_ix_j}$ is a Hermitian matrix, the above equation can be rewritten by applying an eigenvalue decomposition to $G_{x_ix_j}$ as

$$\hat{G}_{y_iy_j} = HAG_{ww}A'H' = H_{yw}G_{ww}H'_{yw}. \tag{3}$$

where the diagonal matrix G_{ww} contains the eigenvalues representing the ranked energy of the modes, and the left eigenvector H_{yw} represents the corresponding ranked modes.

Since only the dominant dynamic contents are of interest, the peak levels of the power-spectral-density (diagonal terms) of $\hat{G}_{y_iy_j}$ can be equivalently reproduced using the superposition of delta functions at the Rossiter frequencies. Therefore, in the time domain, these oscillatory structures are essentially the superposition of Fourier components at these specific frequencies. By retaining only the highest rank-one mode, the reduced order modeling of the flow fields can be expressed as

$$\begin{aligned} \hat{y}(t) &= \bar{y} + \sum_{i=1}^{4}\sqrt{2\hat{G}_{yy}}\sin(2\pi f_i t + \phi_i) \\ &= \bar{y} + \sum_{i=1}^{4}|H_{iyw}|\sqrt{2G_{iww}}\sin(2\pi f_i t + \phi_i), \end{aligned} \tag{4}$$

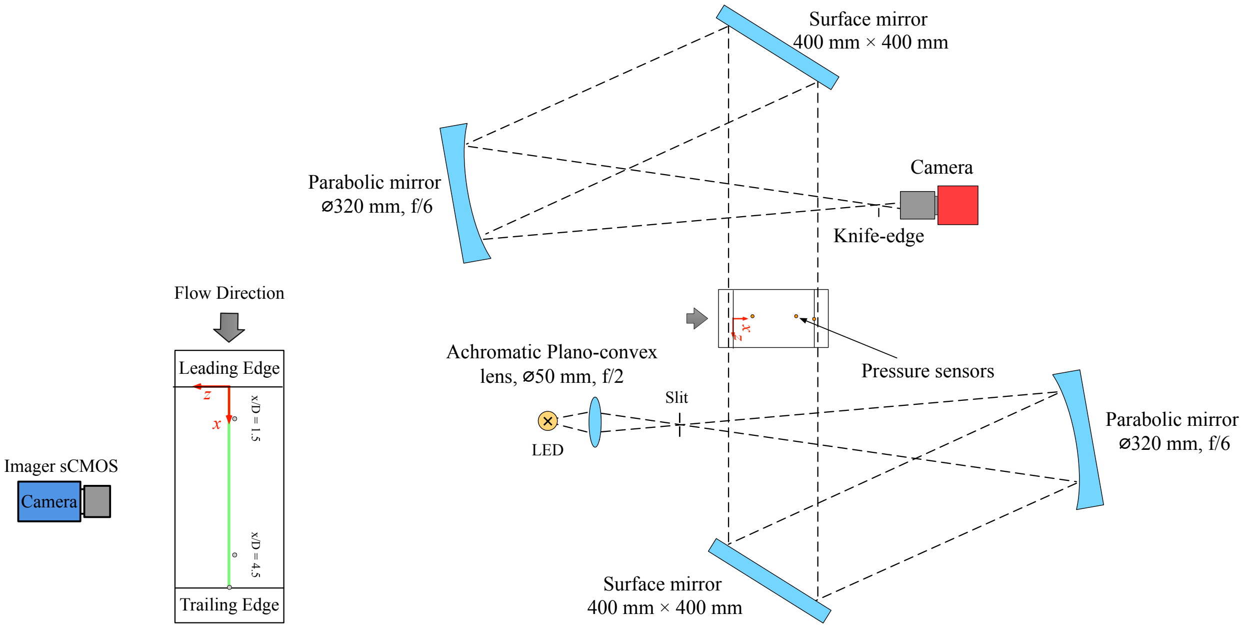

(a) Synchronized PIV and pressure measurements

(b) Synchronized Schlieren and pressure measurements

Figure 1: Experimental arrangement

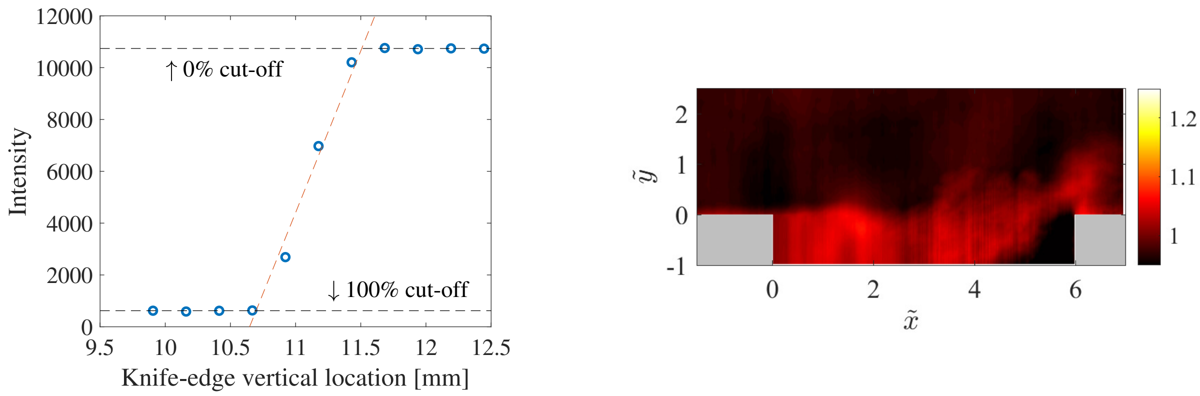

(a) Calibration of quantitative Schlieren

(b) Instantaneous density flow [kg/m^3]

Figure 2: Example of quantitative schlieren. $\tilde{x}$ and $\tilde{y}$ are the nondimensional coordinates.

where $\bar{y}$ is the time-averaged flow field, G_{iww} is the energy of i^{th} mode, f_i is the frequency of the corresponding Rossiter mode, and the initial phase angle ϕ_i is obtained from the phase of the mode in H_{iyw}. This reduced-order reconstruction provides an instantaneous flow field by only using the coherent oscillatory structures, a generic expression for either the velocity or density field.

Results

The sound pressure level (SPL) of pressure fluctuations at three sensor locations are shown in Figure 3. The SPL tends to increase from upstream to downstream, and tonal peaks are observed at all sensor locations. As demonstrated in Zhang *et al.* (2020), due to the dominant global modes of cavity flows, two pressure sensors (the minimum number for a MIMO system) are sufficient for obtaining the dynamically coherent modes (almost identical). In the current case, the FF and AF sensors are chosen as the inputs X. When the downsampled pressure data at the third sensor (AW) are chosen as the output, SAMM provides a reduced-order model of the pressure signature on the cavity aft wall. Figure 4 shows the reduced-order reconstruction of the AW pressure spectra using Equation 3 by only keeping the rank-1 eigenvalue and eigenvector. The rank-1 mode contains most of the energy. Therefore, the tonal peak levels are closely matched at Rossiter frequencies, while the broadband frequencies are less accurate. This is an inherent limitation of SAMM because only the tonal components of the inputs and outputs exhibit strong correlations. Thus the embedded information in the output can be recovered.

The velocity modes corresponding to the first four Rossiter frequencies, with the $4th$ mode at approximately 2 kHz, are provided in Figure 5. These modes are almost identical to the Spectral POD ((Lumley, 1967; Towne *et al.*, 2018))

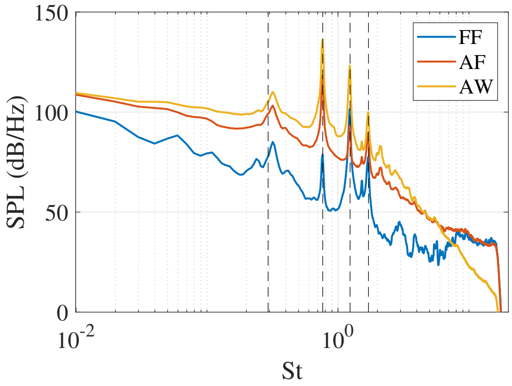

Figure 3: Pressure spectra (reference pressure: 20 μPa). FF: front floor, AF: aft floor, AW: aft wall. The dashed lines indicate the estimated Rossiter frequencies using $St = fL/U_\infty = (n-\alpha)/(1/\kappa + \mathrm{Ma}_\infty/\sqrt{1+(\gamma-1)\mathrm{Ma}_\infty^2/2})$ (Heller *et al.*, 1971), where $\alpha = 0.38$ and $\kappa = 0.65$.

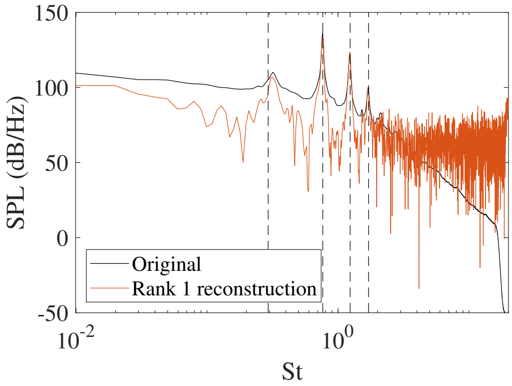

Figure 4: Reduced order reconstruction of the pressure spectra on the cavity aft wall. The dashed lines indicate the estimated Rossiter frequencies.

modes from the time-resolved PIV measurements sampled at 16 kHz (Zhang *et al.*, 2020). Both u and v modes exhibit the typical characteristics of the shear layer modes induced by the Kevin-Helmholtz instability. As frequency increases, the wavelength of the coherent structures becomes smaller. The modal shapes have more noise in modes 1 and 4, which are due to the lower signal-to-noise ratio compared with modes 2 and 3 (referring to Figure 4 for the tonal peak levels). It should be noted that, besides the modes shown in this paper, modes of any flow quantity derived from known parameters can be obtained using the same method.

Phase information is needed to link the velocity field to the density field from two independent measurements. Because the phase information is preserved in the cross-spectral density G_{xy} between the input and output, this guarantees the phase of output Y (velocity, density, or pressure) with respect to the input X (pressure) is consistent even though these two experiments are performed independently (assuming stationarity). Then Equation 4 can be used to reconstruct the temporal evolution of each mode only using the corresponding mode. For example, the spanwise vorticity and density fields at the same time instance in each mode cycle are produced and are compared in Figure 6. In addition, the level of the pressure fluctuations of each Rossiter mode at three sensor locations at the same time instance are shown. The density modes from the quantitative Schlieren are necessarily integrated along the spanwise width of the shear layer, unlike the velocity modes obtained in the central plane. Another difference is that larger-scale waves radiating from the cavity trailing edge to the upstream are also observed, which are not observed in the velocity modes.

In Figure 6, for the evolution of flow fluctuation in the time domain, the time instance is selected at a phase of 0, $\pi/2$, π, and $3\pi/2$, respectively, from left to right. For Rossiter mode 1 (Figure 6a), there is only one large positive vortical structure located at $\tilde{x} = 4$ at phase 0. At this time, a compression region (positive density fluctuation) of the flow is observed in the vicinity of the cavity aft wall. When this vortical structure travels to location $\tilde{x} = 5$, a new stretched counter-rotating vortical structure forms in the middle of the cavity. As the core of the vortical structure with positive vorticity approaches the aft wall, an expansion region (negative density fluctuation) is observed near the cavity aft wall. The amplitude of the pressure fluctuation is near its maximum at phases $\pi/2$ and $3\pi/2$ when the aft wall experiences something between compression and expansion. The aft wall shows a positive pressure fluctuation when the positive vorticity is approaching and vice versa. The flow behavior is 180° out of phase in the latter two time instances.

For Rossiter mode 2 (Figure 6b), the St is more than twice that of the first mode, and there are more vortical structures co-existing in the cavity. The border of compression and expansion regions almost coincides with the core of each vortical structure. Consistent with the flow features in Rossiter mode 1, expansion occurs when a positive vorticity is followed by a negative vorticity in the shear layer. Again, expansion of the flow is associated with positive pressure fluctuations on the cavity surface and vice versa. Although Rossiter mode 2 is the dominant mode at $\tilde{x} = 4.5$ and the aft wall, the Rossiter mode 2 level is the lowest among the Rossiter modes at $\tilde{x} = 1.5$ location (Figure 3). This implies this location is close to an acoustic node. Therefore, the pressure fluctuation of Rossiter mode 2 is lower than other modes at the $\tilde{x} = 1.5$ location.

As the frequency increases in higher Rossiter modes, more vortical structures are present inside the flow field, and the vortical structures become more compact. The fluctuation of the spanwise vorticity is initially stronger in the cavity's front half and then decays as the shear layer travels downstream. By tracing the location of vortex cores, the trajectory is slightly above the cavity trailing edge for Rossiter modes 2-3 (partially escaping), while the vortical structure is at almost the same level as the trailing edge for Rossiter mode 1. Comparing the background pattern of the density fields for different Rossiter modes, the wavelength is independent of St, which is approximately $3.1D$. These waves have a traveling speed close to the speed of sound, indicating that these waves captured in the Schlieren are acoustic waves emanating from the cavity trailing edge. It should be noted that the current method only demonstrates the relationship between velocity, density, and pressure in a reduced-order manner. However, the real flow field is a superposition of all modes and broadband turbulence.

Conclusions

Two experiments, PIV and quantitative Schlieren, are performed independently, along with fluctuating surface pressure measurements inside a cavity flow at Mach 0.6. Both PIV and Schlieren data are sampled at a significantly lower rate than

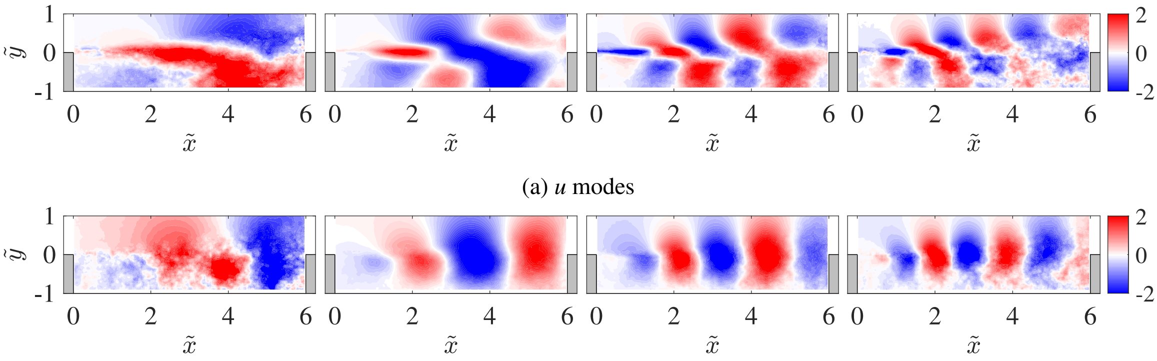

(a) u modes

(b) v modes

Figure 5: Velocity modes for the first four Rossiter modes at Mach 0.6 obtained from SAMM.

the Nyquist frequency that is required to resolve the flow dynamics, while the surface fluctuating pressure measurements are time-resolved. Utilizing SAMM, the embedded information of the flow dynamics in the PIV and Schlieren data are recovered, which leads to the reduced-order reconstruction of the velocity and density flow fields in the time domain.

The velocity modes show the expected characteristics of the shear layer, while the coherent structures of the density modes are confined to spanning the shear layer across the cavity opening due to the integrative nature of Schlieren. In addition, acoustic waves traveling upstream from the cavity trailing edge as the feedback mechanism is observed in the density modes, which is not observable in the velocity modes. Because the phase information is contained in the cross-spectra between the inputs and outputs, the link between the output velocity and density is established through the input pressure. The evolution of the spanwise vorticity fluctuation and density fluctuation in the time domain for each Rossiter frequency is compared with the pressure fluctuation on the aft wall. The expansion and compression regions of the flow field can be identified, along with the coherent vortical structures in the shear layer. The relationship between these flow features and the vortical structures is revealed and is consistent for all Rossiter frequencies.

This study extended the use of SAMM to provide an alternative way to study the high-frequency dynamics of the coherent structures in the flow field. The reduced-order reconstruction isolates the flow component at different frequencies. Interestingly, the relationship between the flow structure and the pressure signature can be utilized for closed-loop control, which will be further explored in future work.

Acknowledgment

This research was supported by the US Air Force Office of Scientific Research (Grant FA9550-22-1-0013, monitored by Dr. Gregg Abate). The authors also gratefully acknowledge fruitful conversations with Prof. Zhao Pan.

REFERENCES

Adrian, Ronald J. 1979 Conditional eddies in isotropic turbulence. *The Physics of Fluids* **22** (11), 2065–2070.

Durgesh, V. & Naughton, J. W. 2010 Multi-time-delay lse-pod complementary approach applied to unsteady high-reynolds-number near wake flow. *Experiments in Fluids* **49**, 571–583.

Garg, S. & Cattafesta III, L. N. 2001 Quantitative schlieren measurements of coherent structures in a cavity shear layer. *Experiments in Fluids* **30** (2), 123–134.

Griffin, John, Schultz, Todd, Holman, Ryan, Ukeiley, Lawrence S. & Cattafesta, Louis N. 2010 Application of multivariate outlier detection to fluid velocity measurements. *Experiments in Fluids* **49** (1), 305–317.

Heller, H.H., Holmes, D.G. & Covert, E.E. 1971 Flow-induced pressure oscillations in shallow cavities. *Journal of Sound and Vibration* **18** (4), 545–553.

Lumley, J. L. 1967 The structure of inhomogeneous turbulent flows. In *Atmospheric turbulence and radio propagation* (ed. A. M. Yaglom & V. I. Tatarski), pp. 166–178.

Murray, Nathan E. & Ukeiley, Lawrence S. 2003 Estimation of the flowfield from surface pressure measurements in an open cavity. *AIAA Journal* **41** (5), 969–972.

Murray, Nathan E. & Ukeiley, Lawrence S. 2006 An application of gappy pod: For subsonic cavity flow piv data. *Experiments in Fluids* **42** (1), 79–91.

Rockwell, D. & Naudascher, E. 1978 Review—self-sustaining oscillations of flow past cavities. *Journal of Fluids Engineering* **100** (2), 152–165.

Rossiter, J. E. 1964 Wind-tunnel Experiments on the Flow over Rectangular Cavities at Subsonic and Transonic speeds. *Tech. Rep.*. Aeronautical Research Council Reports and Memoranda, no. 3438.

Tam, Christopher K. W. & Block, Patricia J. W. 1978 On the tones and pressure oscillations induced by flow over rectangular cavities. *Journal of Fluid Mechanics* **89** (2), 373–399.

Taylor, J. A. & Glauser, M. N. 2004 Towards Practical Flow Sensing and Control via POD and LSE Based Low-Dimensional Tools. *Journal of Fluids Engineering* **126** (3), 337–345.

Tinney, C. E., Coiffet, F., Delville, J., Hall, A. M., Jordan, P. & Glauser, M. N. 2006 On spectral linear stochastic estimation. *Experiments in Fluids* **41** (5), 763–775.

Towne, Aaron, Schmidt, Oliver T. & Colonius, Tim 2018 Spectral proper orthogonal decomposition and its relationship to dynamic mode decomposition and resolvent analysis. *Journal of Fluid Mechanics* **847**, 821–867.

Venturi, Daniele & Karniadakis, George EM 2004 Gappy data and reconstruction procedures for flow past a cylinder. *Journal of Fluid Mechanics* **519**, 315–336.

Zhang, Yang, Cattafesta, Louis N. & Ukeiley, Lawrence 2020 Spectral analysis modal methods (SAMMs) using non-time-resolved PIV. *Experiments in Fluids* **61** (11).

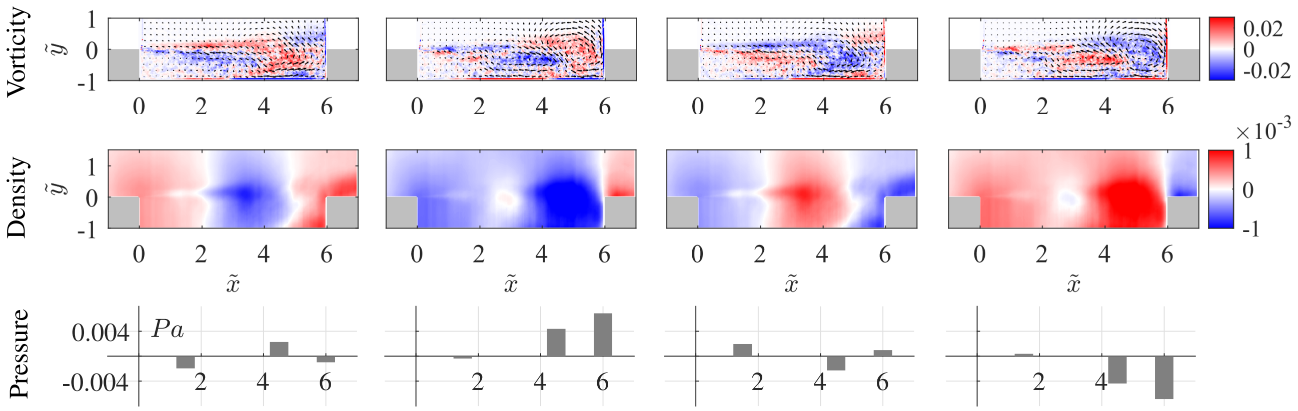

(a) Rossiter mode 1, $St = 0.32$

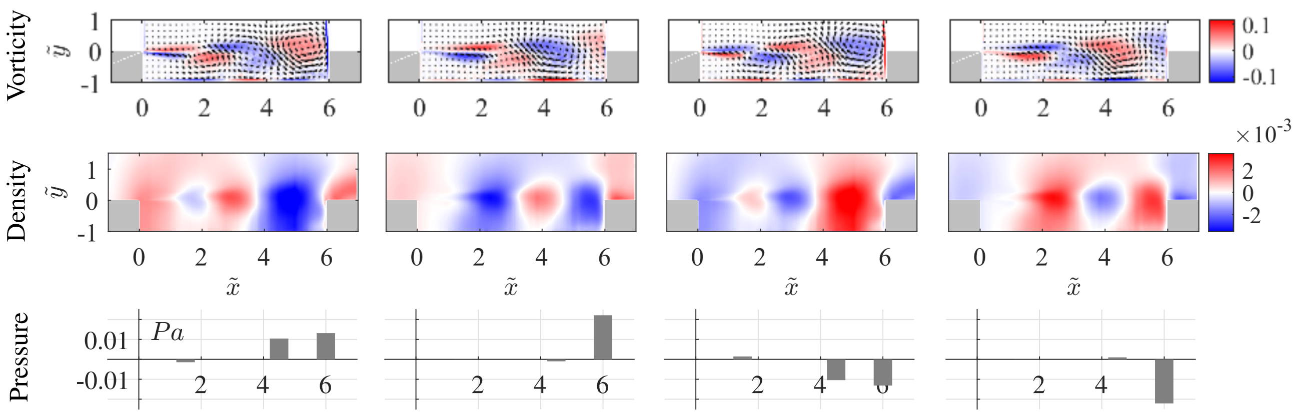

(b) Rossiter mode 2, $St = 0.76$

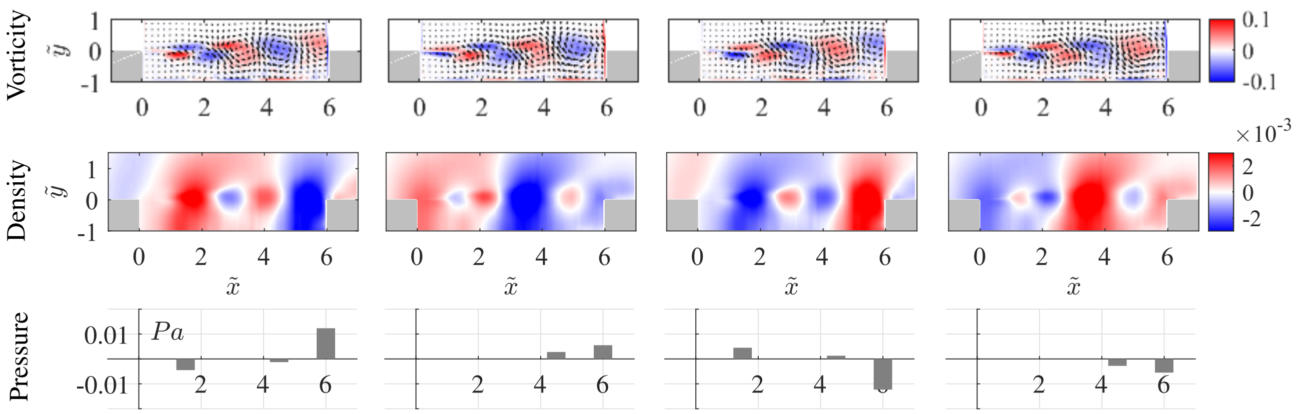

(c) Rossiter mode 3, $St = 1.23$

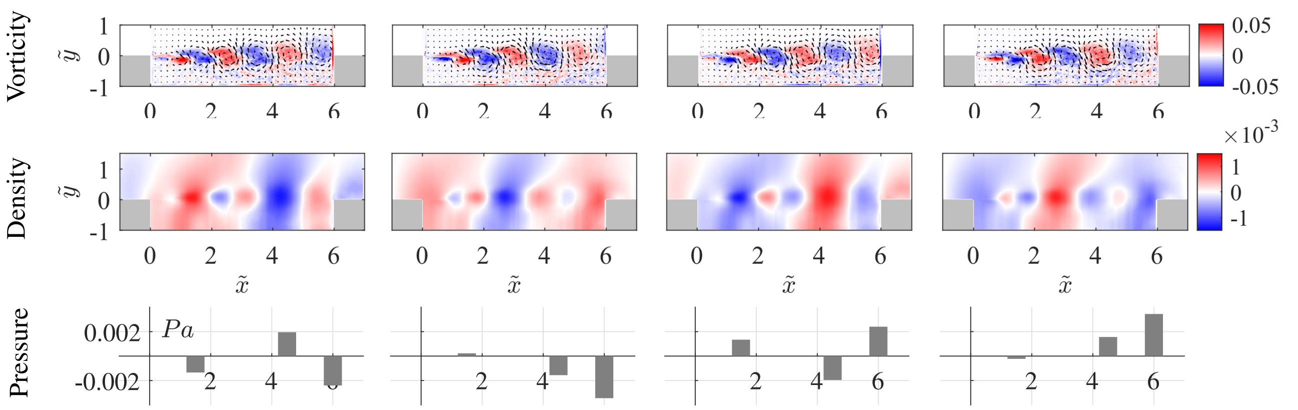

(d) Rossiter mode 4, $St = 1.70$

Figure 6: Temporal evolution of flow fluctuation at different phases within a cycle for different Rossiter frequencies. The phases are 0, $\pi/2$, π, $3\pi/2$ from left to right. From top to bottom in each sub-figure are spanwise vorticity, density, and pressure. Vectors are superimposed on the contour of nondimensional spanwise vorticity $\omega_z D/U_\infty$.